Experimental and numerical study of the response of the offshore combined wind/wave energy concept SFC in extreme environmental conditions

Constantine Michailides, Zhen Gao and Torgeir Moan

Centre for Ships and Ocean Structures (CeSOS), Centre for Autonomous Marine Operations and Systems (AMOS), Department of Marine Technology,
Norwegian University of Science and Technology (NTNU)
Otto Nielsens vei 10, NO-7491, Trondheim, Norway
Email: constantine.michailides@ntnu.no (corresponding author); zhen.gao@ntnu.no; torgeir.moan@ntnu.no

Abstract

This paper deals with an experimental study of the survivability of the offshore combined concept Semisubmersible wind energy and Flap-type wave energy Converter (SFC) and with comparisons of the experimental data with numerical predictions. The SFC is a combined energy concept consisting of a braceless semisubmersible type floating wind turbine and three fully submerged rotating flap-type Wave Energy Converters (WECs). In order to study the survivability of the concept the focus is on extreme environmental conditions. In these conditions the SFC will not produce wind or wave power; the wind turbine is parked with the blades feathered into the wind and the WECs are released to freely rotate about their axis of rotation. Firstly the development and set-up of the physical model are presented. Static, quasi-static, decay, regular waves and irregular waves with wind loading tests are conducted on an 1:50 scale physical model. Aligned and oblique wave with wind loading conditions are considered. Measured variables that are presented include motions of the semisubmersible platform in six rigid body degrees of freedom, rotation of the flap-type WECs, tension of mooring lines, internal loads of the arms that connect the flap with the pontoon of the platform and tower base bending moment. The experimental data are compared with numerical predictions obtained by a fully coupled numerical model. The comparison is made at model scale. A good agreement between experimental data and numerical predictions is observed confirming the accuracy of the numerical models and tools that are used. The discrepancy between numerical and experimental results is smaller for regular than irregular waves. Compared to oblique conditions a better agreement between experimental and numerical results is obtained for the case of aligned wave and wind loadings. The results obtained demonstrate the good performance of the SFC concept in extreme environmental conditions. No strong nonlinear hydrodynamic phenomena are observed in the tests.

Keywords: Offshore combined energy concepts; Marine renewable energy structures; Semisubmersible floating wind turbine; Flap-type wave energy converters; Physical model testing; Survivability.

1. Introduction

Offshore renewable energy systems are expected to significantly contribute in the coming years to the energy security targets worldwide. In recent years, the technology of offshore wind turbines has been rapidly developed mainly for fixed-bottom concepts and shallow waters. However, since the higher wind potential is found in deep seas (approximately for larger depths than 100 m) the development of floating wind turbines has been desired. Different floating support platform configurations are possible for use with offshore wind turbines [1,2] such as tension leg platform [3,4], spar [5,6], barge [7] and semisubmersible [8,9,10,11]. Meanwhile, significant opportunities and benefits have been identified in the area of ocean wave energy and many different types of Wave Energy Converters (WECs) have been proposed by a great number of researchers [12,13]. Still, the technology of WECs cannot be considered mature enough for large-scale commercial deployment mainly due to survivability related problems that render the profitability of WECs questionable. One major category of WECs is the rotating flap [12,13,14]. Experimental investigation of the performance of either offshore wind turbines or WECs has been reported so far by various researchers [15,16,17,18,19,20,21,22,23].

For both offshore wind energy and ocean wave energy there is a need for reduction of costs and efficient use of the ocean space. It might be beneficial to combine these energy systems of different technology in a farm configuration or in one platform. The integration of wind and wave energy systems in a single platform for exploitation of offshore wind and wave energy resources should be assessed and evaluated through appropriate numerical and experimental models. Recently, EU research projects have been introduced in order to accelerate the development of combined offshore energy systems [24,25,26,27,28]. Several researchers studied combined concepts utilizing different floating support platform and type of WECs [29,30,31].

In the EU project MARINA Platform [24] the evaluation of multi-purpose platforms for marine renewable energy has been identified considering five simplified criteria. These criteria are: (a) cost of energy, (b) constructability, (c) installability, (d) operation and maintenance and (e) survivability. Based on the five aforementioned criteria three concepts have been selected and studied numerically and experimentally under operational and extreme conditions. These combined concepts are the Semisubmersible wind energy and Flap-type wave energy Converter (SFC), the Spar Torus Combination

(STC) [32] and an array of oscillating water columns in a V-shaped concrete large floating platform and one wind turbine combination [33]. The combined concept SFC consists of a braceless semisubmersible platform consisting of four columns and three fully submerged pontoons, a 5 MW wind turbine, three fully submerged flap-type WECs and a mooring line system [34,35].

In the present paper, experimental data of the combined wind/wave energy concept SFC in extreme environmental conditions are presented and compared with predictions obtained by a numerical analysis model. The examined response data are the motions of the semisubmersible platform in six degrees of freedom, rotation of the flap-type WECs, tension of mooring lines, internal loads of the arms that connect the rotating flap with the pontoon of the platform and tower base bending moment of the wind turbine. The SFC is in a survival mode. The wind turbine is parked, the Power Take-Offs (PTOs) are released and the WECs can freely rotate; the SFC is not producing power. The experimental basin, test set-up and different parts of the SFC physical model are described. Afterwards, data obtained by static, quasi-static, decay, regular waves and irregular waves with wind loading tests are presented and compared against predictions obtained with the use of a numerical model. The tension of mooring line and tower base bending moment are not affected by the resonance of the rotation of WECs. The (linear) numerical model predicts the internal loads of the arms of the WECs with an acceptable accuracy. Irregular waves with wind loading tests are conducted subjected to aligned and oblique conditions. Compared to oblique wave with wind loading, better agreement between experimental and numerical data is obtained for the case of aligned conditions. The results obtained demonstrate the good performance of the SFC concept in extreme environmental conditions.

2. Physical model and test set-up description.

In the present section the physical model and the test set-up are described. More specifically, this includes the description of the: (a) experimental basin, (b) different parts of the physical model of SFC, (c) measurement sensors and (d) test conditions.

The tests have been conducted in the Hydrodynamic and Ocean Engineering Tank in Ecole Centrale Nantes (ECN), France, which allows the testing of wave and wind loading features. The basin is 50 m long (wave direction), 30 m wide and 5 m deep. A wavemaker consisting of 48 independent flaps allows the creation of regular and irregular directional waves up to 1 m height with wave period in the range 0.5~5 sec (both in model scale). Moreover, a wind generation system [36] that is composed of eight centrifugal fans placed on the side of the wave basin produces airflow and allows the experimental

investigation of offshore wind turbines. The airflow is conducted via flexible air ducts to the centre of the basin by means of a blowing nozzle with dimensions 2.80 m x 2.80 m. The nozzle is placed at the end of the flexible air ducts in order to homogenize the outflow. The wind generation system is capable for generating wind speed up to 10 m/sec in model scale. A sketch of the plan view of the basin as well as of the arrangement of SFC during the tests is presented in Figure 1.

Properties of the prototype SFC can be found in [34,35]. The physical model of SFC has been built in an 1:50 scale. Froude laws of similitude have been used for the physical modelling of the properties of the platform and rotating flap-type WECs (Table 1). In Figure 2 an artistic 3D view of SFC (Fig. 2a) and the physical model of SFC placed into the basin (Fig. 2b) are presented; in the same figure the wind generation system can be seen. In Figure 3 dimensions of the scale model are presented. An overview of the scale model properties of different parts of the SFC are presented in Table 2. For the WECs the x'x' local axis is aligned with the axis of rotation of WEC while y'y' axis is normal to the axis of rotation.

[Figure 1]

[Figure 2]

[Figure 3]

[Table 1]

[Table 2]

With regard to the platform, all the side walls of the pontoons of the platform have been built with wood and are internally filled with foam and steel bars for achieving the required moment of inertia. The upper part of the side columns of the platform has been built with synthetic glass while the lower part close to the intersection with the pontoons has been built with 3D printed foam. Special attention has been paid by the technicians and researchers of ECN to ensure water tightness of the physical model for limiting the risk of any kind of leaks. A video motion capture system (Qualisys motion capture system) with the use of passive markers (Figure 4) has been used in order to measure the motions of the platform in six degrees of freedom. It should be noted that for all the measurements (wave elevation, internal loads, motions etc.) the sampling rate of the sensors is 120 Hz.

[Figure 4]

The physical model of each WEC consists of one fully submerged flap, two arms and one axis of rotation (shaft). The flap has an elliptical shape with major axis equal to 0.14 m and minor axis equal to 0.07 m. The major axis of the flap has direction that coincides with the direction of the vertical Z axis of the global coordinate system. The length of each flap is 0.4 m. The rotating flap has been built with synthetic foam. Each flap is connected with the pontoon of the platform through two rigid structural arms. The two arms at their lower ends are connected with the axis of rotation of the WEC (Figure 4). The arm and the axis of rotation have been built with titanium. The axis of rotation is directed inside the adjacent side column of the platform through a low bearing. It should be noted that for the purposes of the present paper (survivability testing of SFC with WECs not in operation) only survival wave conditions in which the WECs will not operate and the PTO system is disconnected are considered. This is a similar situation for the wind turbine in extreme wind conditions, where the turbine is parked and doesn't produce any wind power. For the survivability testing of SFC the WECs are released to rotate freely about their axis of rotation. In order to measure the internal loads of the arms of WECs strain gauges have been used. In both arms of WEC2 (Figure 3) load sensors have been used for measuring the axial internal load (FZ) at the upper end of each arm close to the flap. Moreover, strain gauges have been used for measuring the bending moments MX and MY around x'x' and y'y' axes, respectively; the gauges have been placed at the lower end of the arm close to the axis of rotation. The angular motion of the axis of rotation has been measured only for WEC2 with the use of an angular encoder that is placed at the edge of the axis of rotation. For WEC1 and WEC3 only the MX moment has been measured.

The SFC is moored to the basin bottom with the use of three catenary mooring lines made by inox chain. The total length of each mooring line is 16.24 m. The weight in air per unit length of mooring line is 0.061 kg/m and the pretension of the mooring line at the fairlead is 14.23 N. The equivalent horizontal stiffness is 0.225 N/m and the equivalent vertical stiffness is 0.067 N/m. Two load cells have been used for measuring the tension of ML2 and ML3 at their fairlead.

The wind speed is kept constant during the tests. The rotor has the correct mass property and produces the equivalent thrust force in model scale as compared to the NREL 5 MW reference wind turbine. The wind turbine was calibrated in a wind tunnel for determining the input wind speed that is required for obtaining the expected thrust for different blade pitch angles. Based on the results of the calibration the blade pitch angle was set equal to six degrees during the tests. In Table 3 structural properties of different parts of the wind turbine are presented in model scale. The tower has been built with the use of a stainless steel cylinder with diameter 22 mm and thickness 2.3 mm. As far as the tower of the wind turbine,

initially a study was performed in order to select the properties (e.g. diameter, thickness, material) of the tower. The parameters constraining the selection of the properties of the tower are: (a) the first bending frequency of the tower has to be kept in the 'soft-stiff range' 1P and 3P and if possible more close to the 3P value, (b) the total tower mass has to be close to 1.81 kg (in scale model and in order the total mass of the wind turbine to be equal with the total mass of the reference NREL 5MW wind turbine with the use of Froude laws) and (c) the external radius of the tower should be as small as possible since higher wind speeds are used for the selected blade profiles and the wind loading on the tower will be higher in the basin. As far as the blades of the wind turbine, a 0.2 mm thick carbon fibre has been used in order to achieve appropriate mass and length. The blades of the wind turbine are placed in a parked position. In order to measure the fore-aft bending moment at the base of the tower of the wind turbine, MY, a load sensor has been used. Details with regard to the design of the wind turbine are presented in [36]. During the tests the wind speed in one point has been measured. It should be noted that based on calibration of the wind generation system prior the tests of SFC and measurements of the wind speed 2 m behind the blowing nozzle in 17 positions in different heights of the testing area, the distribution of the mean wind speed over the testing area is uniform and the turbulence intensity is lower than 3% [36].

[Table 3]

As far as the environmental conditions, two wave gauges (WG1 and WG2) have been used for measuring the water free surface elevation and a wind load cell (sonic anemometer) has been used for measuring the wind velocity. The rotor thrust has been measured with the use of a force sensor placed at the tower top of the wind turbine. It should be noted that the cables of the sensors are brought to the terminal acquisition through under water.

Different test conditions have been considered in order to study the response of SFC in extreme environmental conditions as well as to calibrate basic structural properties of different parts of SFC. Static, quasi-static and decay tests have been performed in order to estimate basic properties of the physical model of the SFC. Based on static tests the draft of the semisubmersible platform has been estimated. With the use of quasi-static tests the equivalent stiffness and pretension of the mooring lines are estimated. It is noted that the mooring stiffness is properly scaled, so that the natural periods of surge, sway and heave obtain values as designed for the prototype SFC. Based on decay tests the natural periods of five degrees of freedom of platform and rotation of WECs and properties with regard to the viscous damping

model are estimated. Afterwards, regular wave tests have been performed for a range of wave frequencies for estimating the Response Amplitude Operators (RAOs) of different response quantities, namely, motions of platform, tension of mooring lines and internal loads of different parts of SFC. Finally, irregular wave with wind loading tests have been performed in order to investigate the response of SFC in extreme environmental conditions. Statistical quantities of time series of responses and spectra are used for comparison between experimental data and numerical predictions. Irregular wave with wind loading tests have been performed for both aligned and oblique conditions.

3. Numerical modeling of the SFC

In the present study a numerical model for the estimation of the response of SFC in time domain is developed and used. The numerical model of the scaled geometry of the SFC has been developed using the software Simo-Riflex (developed by MARINTEK). This tool further extends the capabilities of the stand alone tool Simo [37] and Riflex [38].

The following parts of the SFC: (a) semisubmersible platform, (b) three WECs, (c) wind turbine hub and (d) wind turbine nacelle are modelled through an integrated mass model and are considered as rigid bodies. The arms of WECs, tower, shaft and blades are modelled through distributed mass and are considered as flexible bodies (beam elements). Moreover, the platform contains master and slave nodes. These nodes are used for the simulation of the connection between the platform with: (a) fairlead of mooring lines, (b) arms of WECs at their lower edge and (c) base tower of wind turbine. For the numerical analysis wave loads on the platform and the flap of WECs have been estimated with the use of potential theory and are included in the analysis. In addition the viscous effects are included in the numerical analysis. The viscous loads are accounted in the numerical analysis using Morison elements and drag coefficients for the columns and pontoons of platform as well as for the flap of WECs As far as slender elements of the model (mooring lines and arms of WECs) the Morison equation [39] is used for the calculation of their wave loads. The upper part of flap of WECs may move out of water obtaining non linear behaviour; the associated nonlinear hydrodynamic response due to out of water motion of the upper part of flap is not considered in the present numerical model.

After an appropriate convergence study with regard to the size of the panels of the wet surface of the platform and flap of WECs, hydrodynamic analysis in WAMIT [40] is performed for the calculation of hydrodynamic coefficients in frequency domain. These coefficients are the added mass, radiation damping, hydrostatic stiffness and excitation wave loads. Simo is then used to model the time-domain

hydrodynamic loads on rigid bodies including the first-order wave loads for all rigid bodies and the second-order wave loads for the platform based on Newman's approximation. The mean drift forces are obtained through conservation of momentum. By using the Newman's approximation the slowly-varying drift forces have been calculated [37,41]. For the implementation of the coupled analysis in time domain the hydrodynamic interaction between the different bodies, platform and flaps, numerically can be expressed with coefficients of: (a) added mass, (b) radiation damping and (c) excitation loads. The interaction coefficients of added mass and radiation damping between the different bodies (platform and flaps) are not considered in the analysis due to limitations of the tool Riflex. For the excitation wave loads the hydrodynamic interaction between the different rigid bodies is taken into account. . It should be noted that the hydrodynamic coefficients of the platform and of the flap of WECs are calculated in WAMIT considering that the platform and flap of WECs are in their equilibrium position. Riflex is a nonlinear time domain program with a finite element formulation that can handle large translations and rotations. Riflex has the capability of performing a coupled analysis where one or more rigid-bodies are integrated with a dynamic model of mooring lines and/or arbitrary external forces. For the development of the numerical model a nonlinear finite element formulation of the mooring lines with beams is used [38]. In Table 4 the numerical modelling methods that are used for different parts of SFC are summarised.

[Table 4]

The measured wave elevation of free surface in WG1 is given as input data as dynamic load to the developed numerical model. It is noted that in the present paper the measured time series of shear force response on the tower top in positive X direction have been given as input data in the numerical analysis.

Numerical analysis of SFC is dealt within Riflex and the following equation of motion is solved in time domain:

$$\mathbf{R}^I\left(\mathbf{r},\ddot{\mathbf{r}},\mathbf{t}\right)+\mathbf{R}^D\left(\mathbf{r},\dot{\mathbf{r}},\mathbf{t}\right)+\mathbf{R}^S\left(\mathbf{r},\mathbf{t}\right)=\mathbf{R}^E\left(\mathbf{r},\dot{\mathbf{r}},\mathbf{t}\right) \quad \text{(Eq. 1)}$$

where $\mathbf{R}^I$ is the inertia force vector, $\mathbf{R}^D$ is the damping force vector, $\mathbf{R}^S$ is the internal structural reaction force vector, $\mathbf{R}^E$ is the external force vector and $\mathbf{r},\dot{\mathbf{r}},\ddot{\mathbf{r}}$ are the structural displacement, velocity and acceleration vectors. It is noted that all the force vectors are established by assembly of the element distributions and the specified discrete nodal forces. Equation 1 expresses a nonlinear system of

differential equations due to displacement dependencies in the inertia and the damping forces between the external load vector and the structural displacement and velocity.

4. Static, quasi-static and decay tests

Prior to the tests with wind and wave loadings, various system identification tests have been performed in calm water in order to identify the basic properties of the survivability physical model of SFC.

Static tests have been performed in still water condition in order to determine the draft of the SFC before attaching the mooring lines as well as after attaching them. The draft of the semisubmersible platform of the SFC physical model during the survivability tests is 0.625 m. The upper point of the fully submerged flap of WECs is 0.065 m below the Mean Water Level (MWL).

Quasi-static tests have been conducted by applying forced offsets in surge direction in order to identify the stiffness of the mooring line ML2 by determining the relationship between the surge displacement of the platform and the tension of the mooring line. Different offsets in the surge direction have been applied and the tension is measured. In Figure 5 a comparison of the experimental and numerical mooring line tension as a function of the offset in surge direction is presented. The numerical predictions are in a good agreement with the test data. For large positive offset in X direction the relative difference between experimental and numerical data is 5%. For offsets larger than 0.6 m the ML2 and ML3 start to behave in a non-linear fashion. It should be noted that all the presented values are for the scaled model geometry of SFC.

[Figure 5]

Experimental free decay tests have been carried out for determining the natural periods of five degrees of freedom of the platform surge, sway, heave, roll and pitch. Decay tests for the yaw degree of freedom of the platform have not been conducted. The reason is that it is extremely difficult into the basin the application of an initial offset in this degree of freedom without exciting the other degrees of freedom. Moreover decay tests for the rotation motion of the WEC2 have been conducted. The platform or the WEC2 is deflected to an initial offset position in calm water and then is released to oscillate. The initial offset is representable of the behaviour of the platform of SFC for extreme environmental conditions. It should be noted that attention has been paid to ensure that the examined degree of freedom was excited during the free decay tests without exciting the other degrees of freedom. Using the time series of the

amplitude of the oscillation of the examined degree of freedom the natural period of the motion is estimated based on the first four oscillations. It should be noted that the initial offset values (Table 5) have been selected because it is believed based on numerical analysis that the behaviour of the platform is expected to reach these offset values for extreme environmental conditions. In Table 5 the natural periods of different motions as measured experimentally and calculated numerically are presented for all examined initial offsets. T_{exp} is the measured natural period of the physical model, while T_{num} is the corresponding calculated natural period. For yaw motion only the T_{num} is presented. Moreover, the absolute value of the relative difference, ε (%), (Eq. 2) between the measured experimentally and predicted numerically natural period of each degree of freedom is presented in Table 5. In Table 5 the equivalent linearized damping ratio, ξ_{exp}, as calculated by the experimental decay test curves is presented.

$$\varepsilon = \frac{\left|T_{\exp} - T_{num}\right|}{T_{\exp}} \cdot 100(\%) \qquad \text{(Eq. 2)}$$

[Table 5]

As shown in Table 5 there is a very good agreement between the natural periods as measured experimentally and predicted numerically. The largest difference occurs for sway motion. The differences between experimental data and numerical predictions for sway motion are attributed to the technical uncertainties during the decay tests related with the application of the initial offset of the platform in sway direction without exciting other degrees of freedom. For the other motions the maximum difference is 2.28 % (for $Pitch_2$ decay test).

In Figure 6 a comparison of the time series of decay tests of $surge_2$ (Fig. 6a), $heave_2$ (Fig. 6b), $pitch_1$ (Fig. 6c) and rotation of WEC2 (Fig. 6d) are presented. In the numerical model potential and viscous damping are accounted as well as the damping that is observed by the existence of the mooring lines. For surge motion a small difference is presented between experimental and numerical results in the beginning of the decay tests; after the first oscillation of the platform the two curves obtain exactly the same form. For heave and pitch a very good agreement exists for both the amplitude and period of the oscillations of the motions. With regard to the rotation of WEC2, a very good agreement is presented. For the experimental decay test of rotation of WEC2, only the first three oscillations of the rotation are presented since it was physically very difficult to apply appropriately a large initial rotation offset without exciting other degrees of freedom.

[Figure 6]

5. Regular wave tests

In order to study the response of the SFC in regular waves without wind loading appropriate tests have been performed and the measured data are compared with numerical analysis predictions. Fourteen different wave periods are examined (Table 6). The examined wave height, H, is equal to 0.04 m. The water depth, d, is 5 m. In Table 6 the Ursell number, U, and the ratio of wave height to wavelength, λ, for the characterization of the waves are presented. The Ursell number is defined as the ratio of the nonlinearity to the shallowness of the wave and is given with the following equation:

$$U = \frac{H\lambda^2}{d^3} \qquad \text{(Eq. 3)}$$

The waves propagate in the positive surge direction (+X). The regular wave tests are used for the evaluation of the Response Amplitude Operator (RAO) of motions of the platform, rotation of WEC2, tension of mooring line ML2, internal loads of arms of WEC2 and tower base bending moment of wind turbine.

[Table 6]

In Figure 7 comparisons of the experimental and numerical RAOs of surge (Fig. 7a), heave (Fig. 7b) and pitch (Fig. 7c) of the platform are presented. All the motions of the platform have natural period that is out of the examined wave period range (Table 6). For all the motions a good agreement between experimental and numerical results exists. As the examined wave period increases the amplitude of the surge and heave increases too. For pitch motion an increase of the amplitude up to the T_5 examined period exists; this is attributed to the peak of the first-order hydrodynamic loads close to the period T_5. It should be noted that for sway, roll and yaw very small RAO values are measured experimentally and are attributed to the uncertainties that exist during the tests (e.g. weight of sensors, cables).

[Figure 7]

Figure 8 shows a comparison between experimental and numerical RAO of the rotation of WEC2. The agreement is good. For the rotation of WEC2 the peak is observed for wave period equal to 2.1 sec, which

is close to the measured natural period of rotation of WEC2. The differences between experimental and numerical results become larger in the period range T_{11} ~ T_{13} where the resonance of the rotation of WEC2 exists. The differences are attributed to the uncertainty of the damping model in the numerical analysis. Coupling between rotation of WEC2 and motions of the platform exists. For surge and pitch the differences between experimental and numerical results in the period range 1.9 ~ 2.1 sec are attributed to the resonance of the rotation of WEC2.

Figure 9 shows a comparison between experimental and numerical RAO of mooring line ML2. A good agreement is observed. Moving from 0.709 sec to 1.122 sec an increase of the tension RAO is presented. For larger values a decrease of the tension RAO is observed. The tension RAO of ML2 is affected by the pitch and surge of the platform and is not affected by the rotation of WEC2.

Figure 10 shows experimental and numerical RAO of internal loads of arms of WEC2. FZ1 and FZ2 are the axial forces of the two arms of WEC2, while MX1, MX2, MY1 and MY2 are bending moments of the two arms of WEC2. FZ1 and FZ2 are measured at the upper edge of the arm (close to the flap of WEC2), while MX1, MX2, MY1 and MY2 are measured at the lower edge of the arm (close to the axis of rotation of WEC2). For both arms of WEC2, FZ1 and FZ2 obtain their largest value for period that corresponds to the natural period of the rotation of WEC2. For both FZ1 and FZ2 the calculated with the numerical analysis forces are always larger than the forces measured during the tests. The differences of FZ1 and FZ2 are larger for examined periods close to the resonance period of rotation of WEC2. The increase of the period from T_1 to T_{14} has as a result the increase of the MX1, MX2, MY1 and MY2. For both arms and compared to the MY bending moment, the MX moment is smaller especially for the examined periods that are close to the resonance of the rotation of WEC2. It is clear that the response of the internal loads of arms of WEC2 is affected by the resonance of the rotation of WEC2 and not by the resonance of the platform's motions. It is noted that in order to determine the thickness of the pipe arms that are used in the numerical analysis the measured RAOs of the internal loads of arms of WECs have been used.

[Figure 8]

[Figure 9]

[Figure 10]

In Figure 11 experimental and numerical RAOs of fore-aft tower base bending moment are presented. A good agreement is presented. The patterns of the two curves have similar trends. The peak of the MY occurs at T_3=0.985 sec. The largest difference between experimental and numerical data is 17% for T_3. It should be noted that the largest relative difference is attributed to the difference between experimental data and numerical prediction between the RAO of pitch for the same wave period. The behaviour of the MY of tower is affected mainly by the motions of the platform and is not affected by the resonance of the rotation of WEC2.

[Figure 11]

6. Irregular wave with wind tests in aligned conditions

In order to study the survivability of the SFC irregular wave with wind tests have been conducted for extreme environmental conditions. It is noted that during the tests the wind turbine is placed in a parked condition and the WECs are released to rotate freely about their axis of rotation.

In total twelve extreme environmental conditions, EEC_i, i=1~12, are examined (Table 7). In the same table the turbulence intensity, TI, of the measured wind thrust force is also presented. The environmental conditions correspond to the site no. 14 and site no. 3 of the MARINA platform project [42]. Initially two different environmental cases are examined for each site considering the 50 year maximum return values. The first case corresponds to the condition with maximum wind speed, U_w, (EEC_1 for site no. 3 and EEC_2 for site no. 14) while the second corresponds to the condition with maximum significant wave height, H_s (EEC_3 for site no. 3 and EEC_4 for site no. 14). The rest examined EEC_i, i=5~12, correspond to possible conditions for these two sites based on contour surfaces as presented in [42]. The duration of the tests is 580 sec. The first 70 seconds of the measured data of the tests have not been considered for the post processing. Figure 12 shows the time series of the free surface elevation in WG1 for EEC_2 (Fig. 12a) and the spectra (Fig. 12b) of the surface elevation in WG1 for EEC_2, EEC_3, EEC_4, EEC_6, EEC_9 and EEC_{12}. It should be noted that the time series of the measured surface elevation have been given as input data for the implementation of the numerical analysis in order to have a fair comparison on responses.

[Table 7]

[Figure 12]

[Table 8]

In Table 8 the statistical standard deviation values of experimental and numerical results of surge, heave, pitch and rotation of WEC2 are presented for EEC_i, i=1~12. It should be noted that hereafter the standard deviation, minimum and maximum values of the 510 sec time series for all the examined environmental conditions are symbolized with std, min and max, respectively. Regarding the std (Table 8) the relative difference between experimental data and numerical predictions is between 1.00% and 15.00% for surge, 1.00% and 30.00% for heave, 2.00% and 10.00% for pitch, and 5.00% and 18.00% for rotation of WEC2. For heave motion the large relative difference of std for EEC_9 is attributed to the very small values that the std has. The std of WEC2 rotation as calculated numerically is always larger compared to the std that is calculated experimentally.

In Figure 13 a comparison of statistical max values of surge, heave, pitch and WEC2 rotation between experimental and numerical results for EEC_i, i=1~12, are presented. The largest relative difference between experimental and numerical max value is 11.10% for surge, 20% for heave, 19% for pitch and 18% for rotation of WEC2. For surge, pitch and rotation of WEC2 the numerical model overestimates the max value. The overestimation of the rotation of WEC2 has a mean value equal to 12%. This discrepancy is attributed to the uncertainties related to the damping model that is used in the numerical analysis. The largest max value that is measured experimentally is 0.307 m for surge, 0.103 m for heave, 4.912 deg for pitch and 24.380 deg for rotation of WEC2 for EEC_6, EEC_4, EEC_4 and EEC_4, respectively.

[Figure 13]

In Figures 14 and 15 comparisons of statistical std and max values of tension of ML2, MY of tower, and FZ1 of WEC2 between experimental and numerical results are presented. It is noted that for EEC_1 the response quantities have not been recorded due to technical problems during the execution of the tests. Regarding the std value, the relative difference between experimental and numerical results for tension of ML2 is between 4.00% and 10.00% for EEC_7 and EEC_4, for MY of tower is between 1.00% and 15.00% for EEC_{10} and EEC_6, and for FZ1 of WEC2 is between 6.00% and 19.00% for EEC_{10} and EEC_{12}. The largest max value that is measured experimentally is 26.053 N for tension of ML2, 0.829 Nm for MY of tower and 14.48 N for FZ1 of WEC2 for EEC_6, EEC_4 and EEC_6, respectively. The relative difference of the statistical max value is 9% for tension of ML2 and EEC_4, 16% for MY of tower and EEC_9 and 23% for FZ1 of WEC2 and EEC_3. The FZ1 of WEC2 is overpredicted by the numerical model for all the examined conditions in a mean value equal to 17%; this is observed since the flaps are partially out of the

water for short time duration (less than the 5% of the total height of flap). This non linear behaviour cannot be simulated with the numerical tools that are used.

[Figure 14]

[Figure 15]

In Figures 16 and 17 comparisons of spectra of surge (Fig. 16a), heave (Fig. 16b), pitch (Fig. 16c), rotation of WEC2 (Fig. 16d), tension of ML2 (Fig. 17a), MY of tower (Fig. 17b), FZ1 of WEC2 (Fig. 17c) and MX1 of WEC2 (Fig. 17d) between experimental and numerical results for EEC_2, EEC_3 and EEC_6, are presented. For the motions of the platform and rotation of WEC2 the peaks of the spectra are observed close to the natural frequency of each motion as calculated by the decay tests (Table 5) and close to the frequency of the excitation waves. For surge motion an initial peak is presented close to ω=0.5 rad/sec attributed to the wind excitation loads. As far as the tension of ML2, the peak is presented close to the frequency of the excitation waves for all EEC_i, i=2,3 and 6. Regarding the MY of tower the peaks are presented close to the: (a) natural frequency of pitch, (b) frequency of excitation waves and (c) first bending mode eigenfrequency of the tower. For both FZ1 of WEC2 and MX1 of WEC2 the peak is presented close to the frequency of excitation waves.

[Figure 16]

[Figure 17]

7. Irregular wave tests subjected to oblique wave with wind loading

In order to study the response and examine the survivability of the SFC in extreme environmental conditions in oblique conditions, the wind direction is aligned with the positive X axis and the wave direction is equal to 22.5 deg (Figure 1). In total four extreme environmental conditions, EEC_i, i=1~4, are examined for oblique wave conditions (Table 7).

Figure 18 shows comparisons between experimental and numerical results of statistical max, min and std values of time series of roll (Fig. 18a), pitch (Fig. 18b), yaw (Fig. 18c) and rotation of WEC2 (Fig. 18d). As far as the std of the examined motions, the largest relative difference between experimental data and numerical predictions is 14% for roll and EEC_3, 12% for pitch and EEC_1, 16% for yaw and EEC_1, and 13% for rotation of WEC2 and EEC_1. The largest max and min values that are measured experimentally

are 1.929 deg and -2.070 deg for roll, 3.436 deg and -2.362 deg for pitch, 2.104 deg and -2.432 deg for yaw, and 19.950 deg and -16.190 deg for rotation of WEC2. It is noted that all the largest max and min values are obtained for EEC_4. The largest relative difference between experimental and numerical statistical max and min value is 20% for roll and EEC_2, 28% for pitch and EEC_2, 22% for yaw and EEC_1 and 29% for rotation of WEC2 and EEC_3. Compared to the irregular tests subjected to aligned wave with wind loading the differences between experimental and numerical results are larger for the case of oblique wave conditions. This is attributed to uncertainties with regard to the measured surface elevation that has been used as input for the implementation of the numerical analysis. The max value of pitch and rotation of WEC2 for oblique wave with wind loading is always smaller than the corresponding max value for aligned environmental conditions.

[Figure 18]

Figure 19 shows a comparison of the statistical max, min and std values of tension of ML2 (Fig. 19a), MY of tower (Fig. 19b) and FZ1 of WEC2 (Fig. 19c) between experimental data and numerical predictions. The largest max value that is measured experimentally is 19.3617 N for tension of ML2, 0.5874 Nm for MY of tower and 14.349 N for FZ1 of WEC2. The largest relative difference between experimental and numerical max and min value is 17.72% for tension of ML2, 24.24% for MY of tower and 23.53% for FZ1 of WEC2. Compared to aligned wave with wind loading the relative difference between experimental and numerical results is larger for the case of oblique wave conditions. The numerical model underestimates the MY of tower. For FZ1 the max value is overestimated by the numerical model.

[Figure 19]

8. Conclusions

This paper deals with the behaviour of the combined wind/wave energy concept SFC in extreme environmental conditions based on physical model tests and numerical analysis. The experimental set-up of the physical model of SFC, measurement sensors, test conditions and basic features of the developed numerical model are described.

The response of the SFC in regular waves (with absence of wind loading) is investigated considering fourteen different wave periods. For all the examined motions of the platform and rotation of WEC2 there is a good agreement between the experimental and numerical RAOs. All the motions of the platform have natural period that is out of the examined wave period range. The peak of pitch motion is attributed to the first-order hydrodynamic loads. The peak of the rotation of WEC2 RAO is observed for the natural period of the motion as calculated with the decay tests. The RAOs of tension of mooring line ML2 and tower base bending moment are not affected by the resonance of the rotation of WEC2; the behaviour of these quantities is affected mainly by the pitch and surge motions of the platform and not by the rotation of WECs. The RAOs of internal loads of the arms of WEC2 are affected by this resonance.

The behaviour of the SFC in extreme environmental conditions is studied based on irregular wave with wind loading tests, considering aligned and oblique wave conditions. For aligned conditions twelve extreme environmental conditions are examined. Comparisons of statistical max, min and std values between experimental and numerical results are presented. The max and min values of pitch motion of the platform, rotation of WEC2 and axial force of arms of WEC2 are overestimated by the numerical model. Limited slamming non-linear loading on the flap of WECs is presented. The (linear) numerical model predicts the internal loads of the arms of the WECs with an acceptable accuracy. Compared to oblique wave with wind loading, better agreement between experimental and numerical data is obtained for the case of aligned conditions. The validated results that are obtained confirm the good performance of the SFC concept in extreme environmental conditions.

The presented data can be used for validation of numerical models of multibody offshore energy systems by various researchers. Finally it will be interesting to compare the presented responses obtained by experiments with numerical analysis where the wind loads will be calculated by a stochastic, full-field, turbulent-wind simulator.

Acknowledgements

The authors would like to acknowledge the financial support from the MARINA Platform project (Marine Renewable Integrated Application Platform, Grant Agreement no. 241402) under the European Community FP7 Energy Programme. The financial support for the construction of the physical model of the SFC concept from the MARINA Platform is greatly acknowledged. The contribution of Thomas Soulard and Sylvain Bourdier at ECN to the planning, construction and execution of the model tests is highly appreciated. The financial support from the Research Council of Norway through the Centre for

Ships and Ocean Structures and the Centre for Autonomous Marine Operations and Systems, the Norwegian University of Science and Technology, is also acknowledged.

References

[1] Nejad AR, Bachynski EE, Kvittem MI, Luan C, Gao Z, Moan T. Stochastic dynamic load effect and fatigue damage analysis of drivetrains in land-based and TLP, spar and semi-submersible floating wind turbines. Marine Structures 2015;42:137-153.

[2] Jonkman JM, Matha D. Dynamics of offshore floating wind turbines-analysis of three concepts. Wind Energy 2011;14(4):557–569.

[3] Bachynski EE, Moan T. Design considerations for tension leg platform wind turbines. Marine Structures 2012;29(1):89-114.

[4] Adam F, Myland T, Schuldt B, Großmann J, Dahlhaus F. Evaluation of internal force superposition on a TLP for wind turbines. Renewable Energy 2014;71:271-275.

[5] Karimirad M, Meissonnier Q, Gao Z, Moan T. Hydro-elastic Code-to-Code Comparison for a Tension Leg Spar Type Floating Wind Turbine. Marine Structures 2011;24(4):412-435.

[6] Nava V, Guedes Soares C, Arena F.On the assessment of extreme forces on a floating spar wind turbine, Developments in Maritime Transportation and Exploitation of Sea Resources, C. Guedes Soares and López Peña (Eds.), Taylor & Francis Group, London 2012:553–562.

[7] Lefebvre S, Collu M. Preliminary design of a floating support structure for a 5MW offshore wind turbine. Ocean Engineering 2012;40:15-26.

[8] Robertson A, Jonkman J, Masciola M, Song H, Goupee A, Coulling A, Luan C. Definition of the Semisubmersible Floating System for Phase II of OC4. NREL/TP-5000-60601, National Renewable Energy Laboratory, Golden, CO, U.S.A, 2014.

[9] Luan C, Gao Z, Moan T. Conceptual designs of a 5-MW and a 10-MW semi-submersible wind turbine with emphasis on the design procedure. (Under review).

[10] Karimirad M, Michailides C. V-shaped semisubmersible offshore wind turbine: An alternative concept for offshore wind technology. Renewable Energy 2015;83:126-143.

[11] Roddier D, Cermelli C, Aubault A, Weinstein A. WindFloat: A floating foundation for offshore wind turbines. Journal of Renewable and Sustainable Energy 2010;2(3): 033104-1-033104-34.

[12] Falnes J. A review of wave-energy extraction. Marine Structures 2007;20:185–201.

[13] Falcão A. Wave energy utilization: A review of the technologies. Ren and Sust Energy Reviews 2010;14:899–918.

[14] Kurniawan A, Moan T. Characteristics of a pitching wave absorber with rotatable flap. Energy Procedia 2012;20:134–147.

[15] Coulling AJ, Goupee AJ, Robertson AN, Jonkman JM, Dagher HJ. Validation of a FAST semi-submersible floating wind turbine numerical model with DeepCwind test data. Journal of Renewable and Sustainable Energy 2013;5,023116.

[16] Huijs F, Ridder EJ, Savenije F. Comparison of model tests and coupled simulations for a semi-submersible floating wind turbine. Proc. OMAE, OMAE2014-23217, San Francisco, USA

[17] Myhr A, Nygaard TA. Comparison of experimental and computations for tension-leg-buoy offshore wind turbines. Journal of Ocean and Wind Energy 2015;2(1):12-20.

[18] Kimball RW, Goupee AJ, Coulling AJ, Dahger HJ. Model Test Comparisons of TLP, Spar-buoy and Semi-submersible Floating Offshore Wind Turbine Systems. Transactions TRANS 2014;120.

[19] Robertson AN, Jonkman JM, Goupee AJ, Coulling AJ, Prowell I, Browning J, Masciola MD, Molta P. Summary of conclusions and recommendations drawn from the DeepCwind scaled floating offshore wind system test campaign. Proc. OMAE, OMAE2013-10817, Nantes, France.

[20] Fernandez H, Iglesias G, Carballo R, Castro A, Fraguela JA, Taveira-Pinto F, Sanchez M. The new wave energy converter WaveCat: Concept and laboratory tests. Marine Structures 2012;29(1):58-70.

[21] Flocard F, Finnigan TD. Laboratory experiments on the power capture of pitching vertical cylinders in waves. Ocean Engineering 2010;37:989-997.

[22] Rogne OY, Ersdal S, Moan T. Numerical and experimental investigation of a novel wave energy converter. Proc. OMAE, OMAE2012-83609, Rio de Janeiro, Brazil.

[23] Kelly T, Dooley T, Campbell J, Ringwood JV. Comparison of the Experimental and Numerical Results of Modelling a 32-OscillatingWater Column (OWC), V-Shaped Floating Wave Energy Converter. Energies 2013;6:4045-4077.

[24] MARINA PLATFORM (Online) Available at: http://www.marina-platform.info/index.aspx [Accessed in June 2015].

[25] ORECCA Website. http://www.orecca.eu/. Accessed in June 2015.

[26] TROPOS Website. http://www.troposplatform.eu/. Accessed in June 2015.

[27] H2Ocean Website. http://www.h2ocean-project.eu/. Accessed in June 2015.

[28] MERMAID Website. http://www.mermaidproject.eu/. Accessed in June 2015.

[29] Soulard T, Babarit A, Borgarino B, Wyns M, Harismendy M. C-HYP: A combined wave and wind energy platform with balanced contributions. Proc. OMAE, OMAE2013-10778, Nantes, France.

[30] Aubult A, Alves M, Sarmento A, Roddier D, Peiffer A. Modeling of an oscillating water column on the floating foundation WindFloat. Proc. OMAE, OMAE2011-49014, Rotterdam, Netherland.

[31] Peiffer A, Roddier D, Aubult A. Design of a point absorber inside the WindFloat structure. Proc. OMAE, OMAE2011-49015, Rotterdam, Netherland.

[32] Muliawan MJ, Karimirad M, Moan T. Dynamic response and power performance of a combined spar-type floating wind turbine and coaxial floating wave energy converter. Renewable Energy 2013;50:47–57.

[33] O'Sullivan K, Murphy J. Techno-Economic Optimisation of an Oscillating Water Column Array Wave Energy Converter. Proc. of the 10th European Wave and Tidal Energy Conference, Aalborg, Denmark.

[34] Michailides C, Luan C, Gao Z, Moan T. Effect of Flap Type Wave Energy Converters on the Response of a Semi-submersible Wind Turbine in Operational Conditions. Proceedings of the International Conference on Offshore Mechanics and Arctic Engineering - OMAE, Volume 9B: Ocean Renewable Energy,San Francisco, California, USA, June 8–13, 2014, Paper No. OMAE2014-24065, pp. V09BT09A014, doi:10.1115/OMAE2014-24065.

[35] Gao Z, Moan T, Wan L, Michailides C. Comparative numerical and experimental study of two combined wind and wave energy concepts. Journal of Ocean Engineering and Science 2016;1:36-51.

[36] Courbois A. Etude expérimentale du comportement dynamique d'une éolienne offshore flottante soumise à l'action conjuguée de la houle et du vent. Ph.D. thesis, Ecole Centrale de Nantes 2013 (in french).

[37] MARINTEK. Simo User's Manual 2015. Trondheim, Norway.

[38] MARINTEK. Riflex User's Manual 2013. Trondheim, Norway.

[39] Faltinsen O. Sea loads on ships and offshore structures. Cambridge: Cambridge University Press;1993.

[40] WAMIT. User Manual – program version 6.4 2009 WAMIT Inc. Available at: http:// www.wamit.com. [Accessed in June 2015].

[41] Newman JN. Second-order, Slowly-varying Forces on Vessels in Irregular Waves, In Proc. of Int. Symp. on Dynamics of Marine Vehicles and Structures in Waves, pp. 182-6, Mechanical Engineering Publication Ltd, London, 1974.

[42] Li L, Gao Z, Moan T. Joint Distribution of Environmental Condition at Five European Offshore Sites for Design of Combined Wind and Wave Energy Devices. Journal of Offshore Mechanics and Arctic Engineering 2015;137,031901-1.

Figure Captions

Figure 1. Plan view of the experimental set-up of SFC at ECN

Figure 2. Artistic view of the SFC (Fig. 2a) and the physical model of SFC into the basin (Fig. 2b) (Wind direction is opposite in these two plots)

Figure 3. Plan view of SFC (Fig. 3a), dimensions of the scale model of SFC for different Z levels (Fig. 3b for Z=-0.625 and Fig. 3c for Z=-0.505) and section view of SFC (Fig. 3d) (all measures are in terms of metre)

Figure 4. Physical model of SFC

Figure 5. Tension of mooring line ML2 for different offset in X direction during quasi-static tests

Figure 6. Time series of decay tests measured into basin and calculated numerically of $surge_2$ (Fig. 6a), $heave_2$ (Fig. 6b), $pitch_1$ (Fig. 6c) and rotation of WEC2 (Fig. 6d)

Figure 7. Experimental and numerical RAO of surge (Fig. 7a), heave (Fig. 7b), and pitch (Fig. 7c) of the platform

Figure 8. Experimental and numerical RAO of rotation of WEC2

Figure 9. Experimental and numerical RAO of tension of ML2

Figure 10. Experimental and numerical RAO of FZ1 (Fig. 10a), FZ2 (Fig. 10b), MX1 and MY1 (Fig. 10c), and MX2 and MY2 (Fig. 10d) of WEC2

Figure 11. Experimental and numerical RAO of fore-aft bending moment of tower

Figure 12. Time series of the surface elevation for EEC_2 (Fig. 12a) and spectra (Fig. 12b) of the surface elevation for EEC_2, EEC_3, EEC_4, EEC_6, EEC_9 and EEC_{12}

Figure 13. Statistical experimental and numerical max values of time series of surge (Fig. 13a), heave (Fig. 13b), pitch (Fig. 13c) and rotation of WEC2 (Fig. 13d) for EEC_i, i=1~12

Figure 14. Comparison of statistical std value for EEC_i, i=1~12 of tension of ML2 (Fig. 14a), MY of tower (Fig. 14b) and FZ1 of WEC2 (Fig. 14c)

Figure 15. Comparison of statistical max value for EEC_i, i=1~12 of tension of ML2 (Fig. 15a), MY of tower (Fig. 15b) and FZ1 of WEC2 (Fig. 15c)

Figure 16. Comparison of spectra of surge (Fig. 16a), heave (Fig. 16b), pitch (Fig. 16c) and WEC2 rotation (Fig. 16d) between experimental and numerical results for EEC_2, EEC_3 and EEC_6

Figure 17. Comparison of spectra of tension of ML2 (Fig. 17a), MY of tower (Fig. 17b), FZ1 of WEC2 (Fig. 17c) and MX1 of WEC2 (Fig. 17d) between experimental and numerical results for EEC_2, EEC_3 and EEC_6

Figure 18. Statistical max, min and std values of roll (Fig. 18a), pitch (Fig. 18b), yaw (Fig. 18c) and rotation of WEC2 (Fig. 18d) for EEC_i, i=1~4 subjected to oblique wave and wind conditions

Figure 19. Statistical max, min and std values of ML2 tension (Fig. 19a), MY of tower (Fig. 19b) and FZ1 of WEC2 (Fig. 19c) for EEC_i, i=1~4, subjected to oblique wave with wind loading

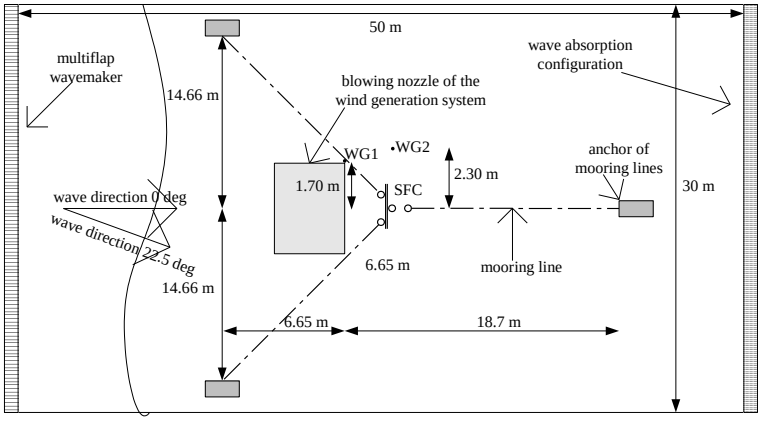

Figure 1. Plan view of the experimental set-up of SFC at ECN

Figure 2. Artistic view of the SFC (Fig. 2a) and the physical model of SFC into the basin (Fig. 2b) (Wind direction is opposite in these two plots)

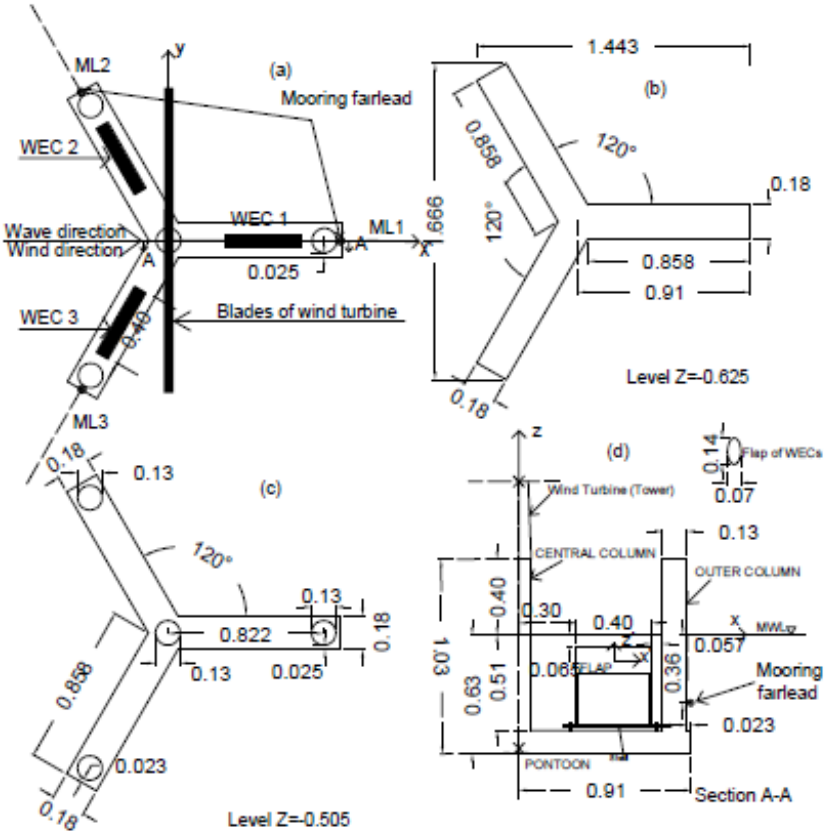

Figure 3. Plan view of SFC (Fig. 3a), dimensions of the scale model of SFC for different Z levels (Fig. 3b for Z=-0.625 and Fig. 3c for Z=-0.505) and section view of SFC (Fig. 3d) (all measures are in terms of metre)

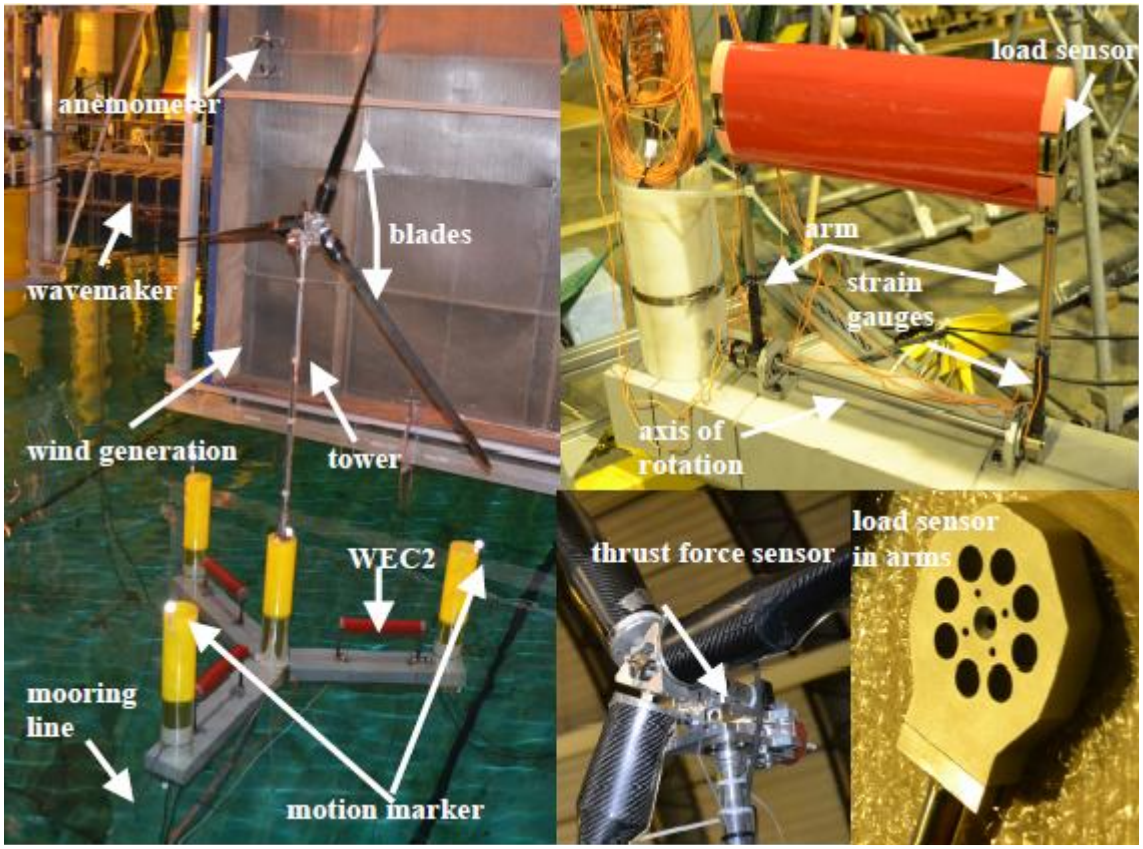

Figure 4. Physical model of SFC

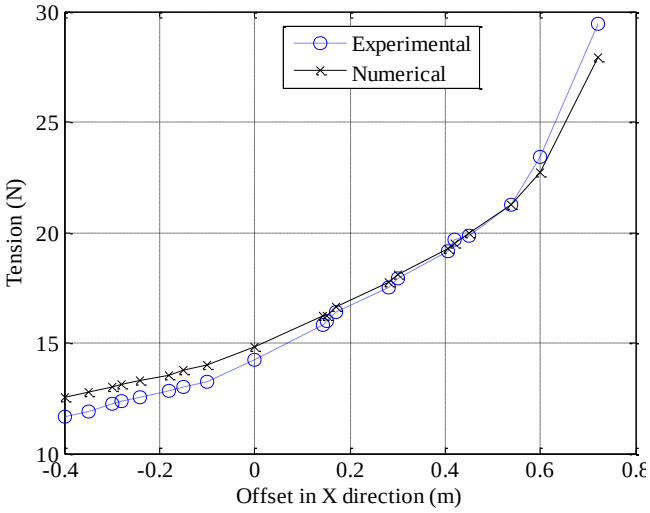

Figure 5. Tension of mooring line ML2 for different offset in X direction during quasi-static tests

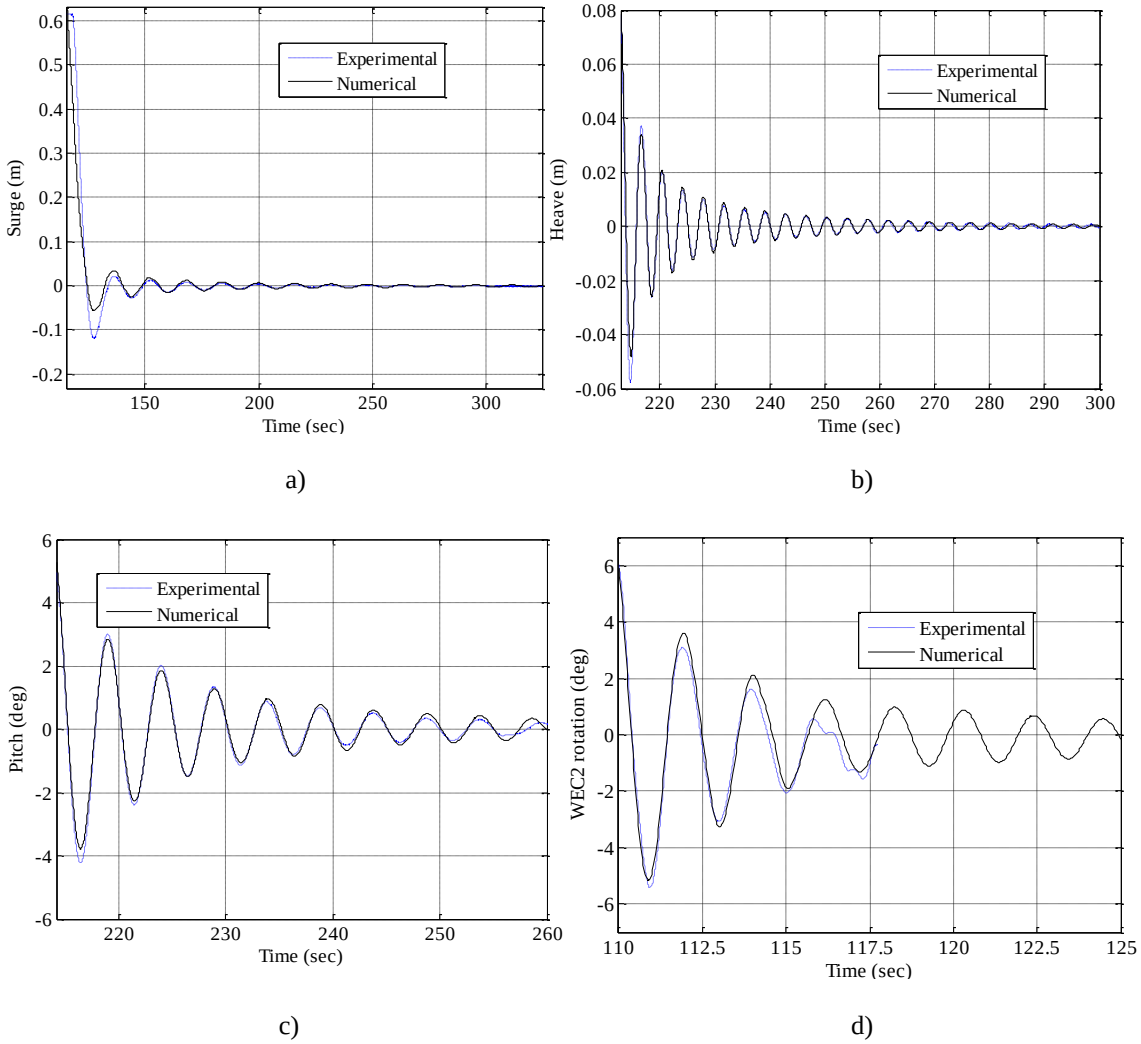

Figure 6. Time series of decay tests measured into basin and calculated numerically of surge$_2$ (Fig. 6a), heave$_2$ (Fig. 6b), pitch$_1$ (Fig. 6c) and rotation of WEC2 (Fig. 6d)

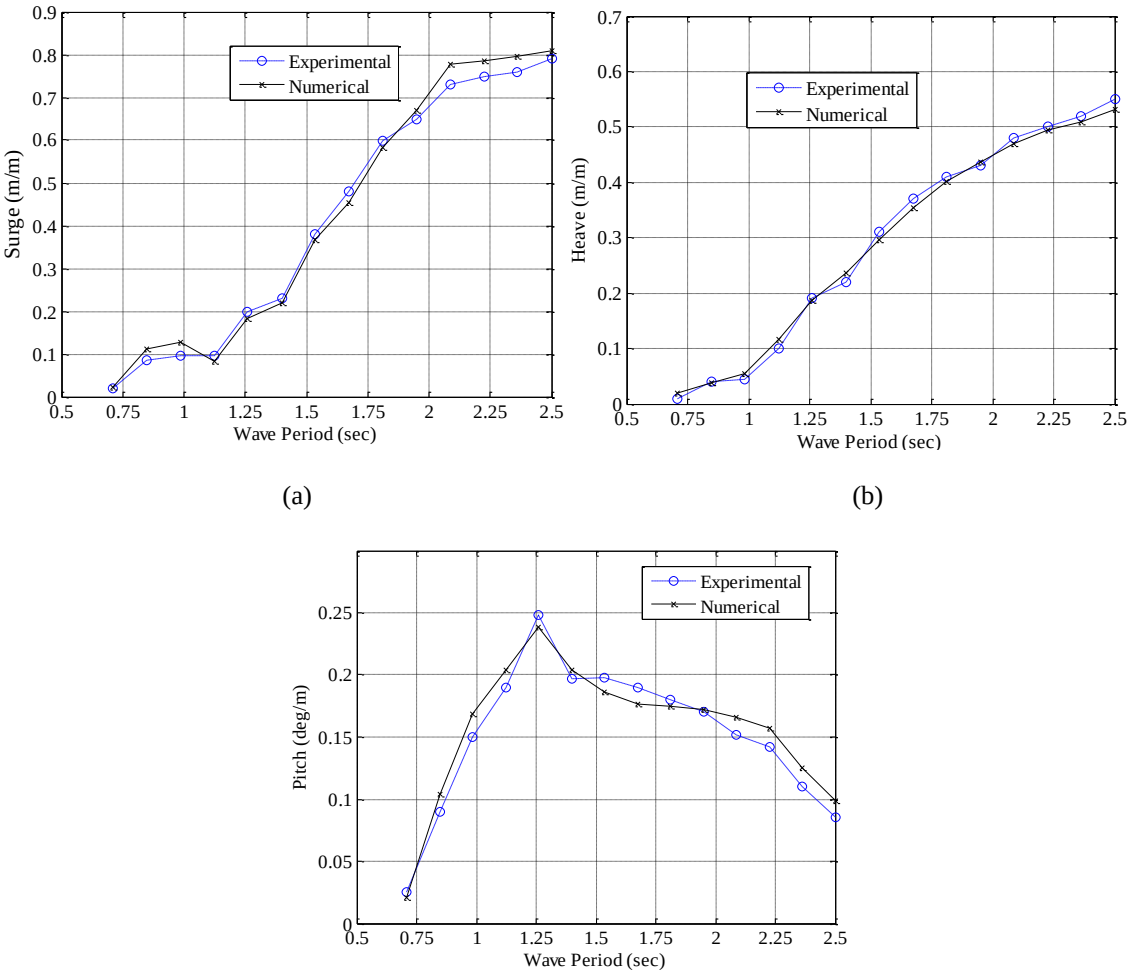

Figure 7. Experimental and numerical RAO of surge (Fig. 7a), heave (Fig. 7b), and pitch (Fig. 7c) of the platform

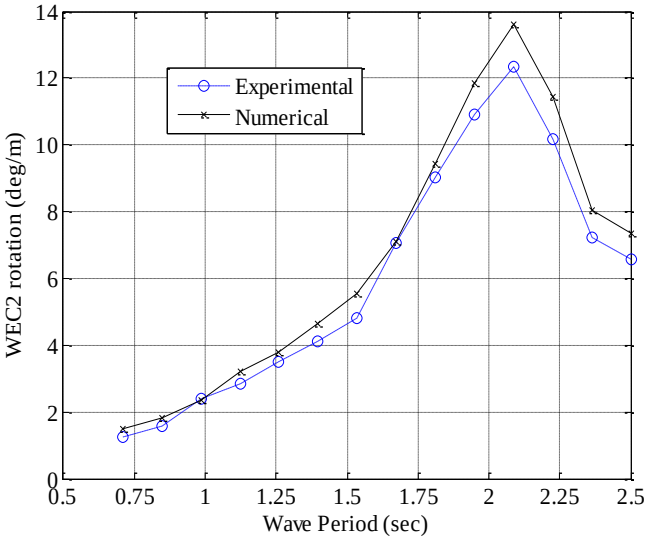

Figure 8. Experimental and numerical RAO of rotation of WEC2

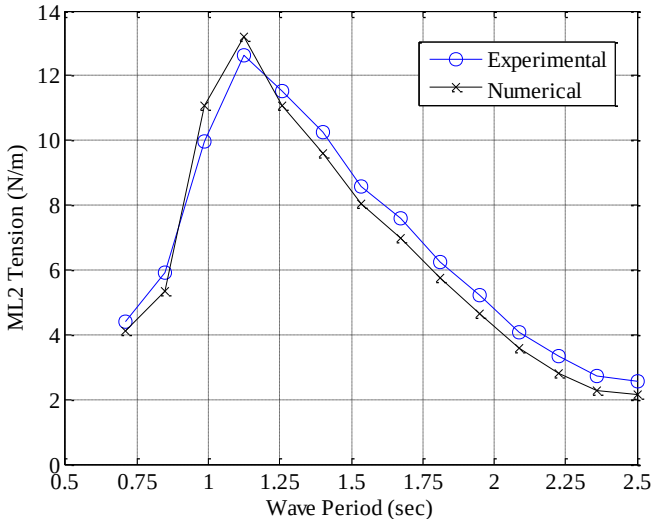

Figure 9. Experimental and numerical RAO of tension of ML2

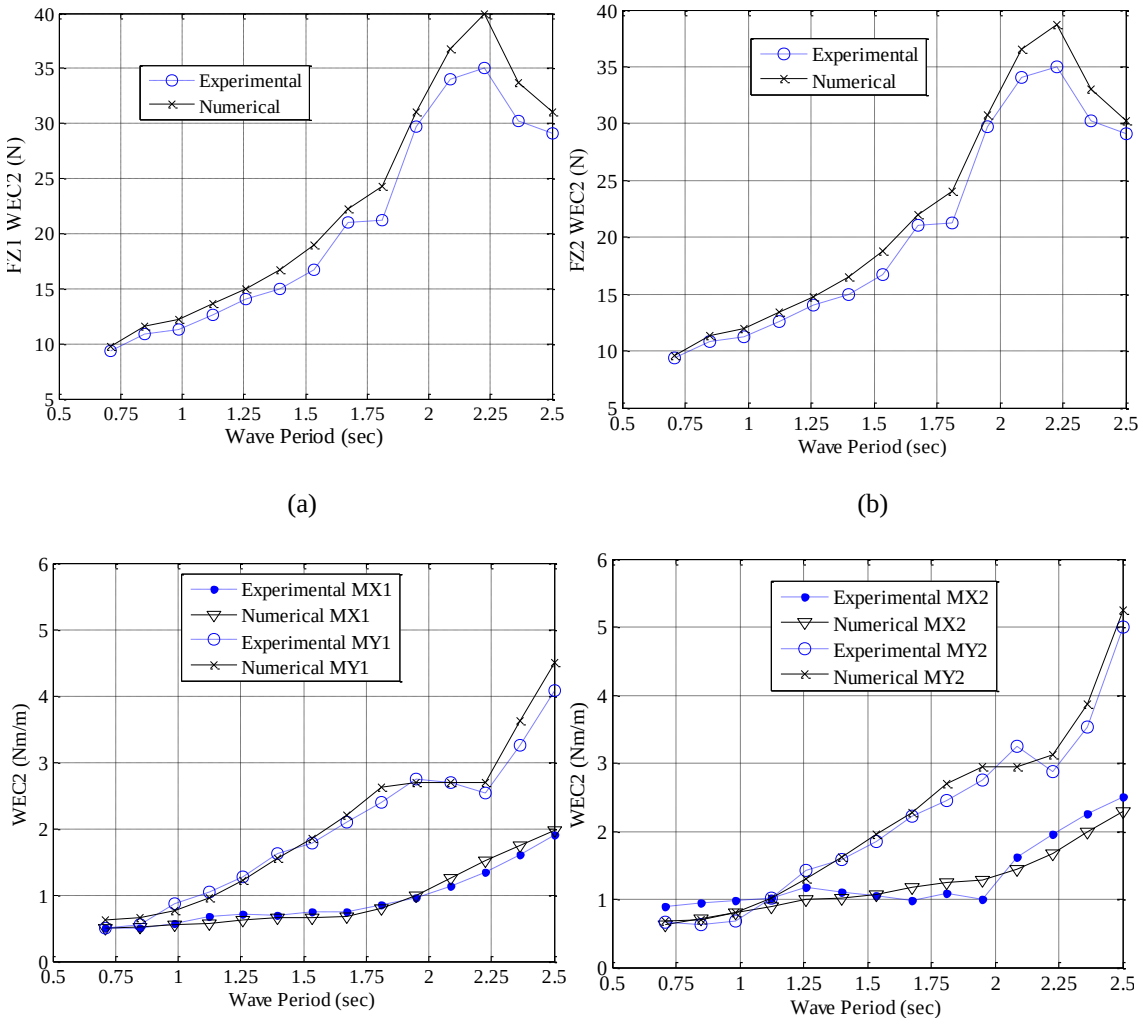

Figure 10. Experimental and numerical RAO of FZ1 (Fig. 10a), FZ2 (Fig. 10b), MX1 and MY1 (Fig. 10c), and MX2 and MY2 (Fig. 10d) of WEC2

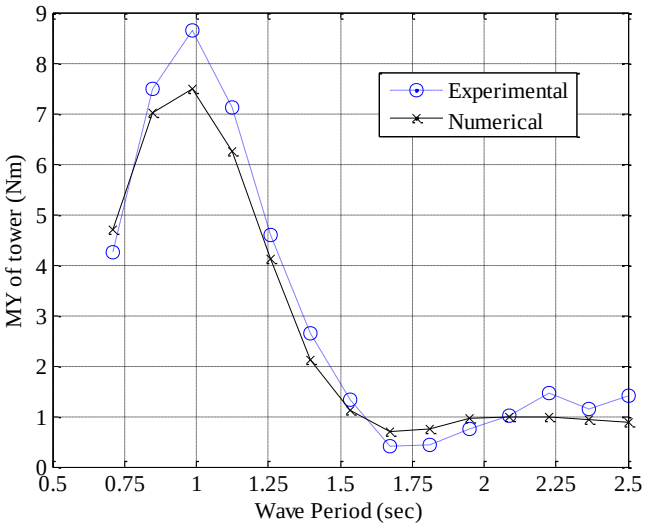

Figure 11. Experimental and numerical RAO of fore-aft bending moment of tower

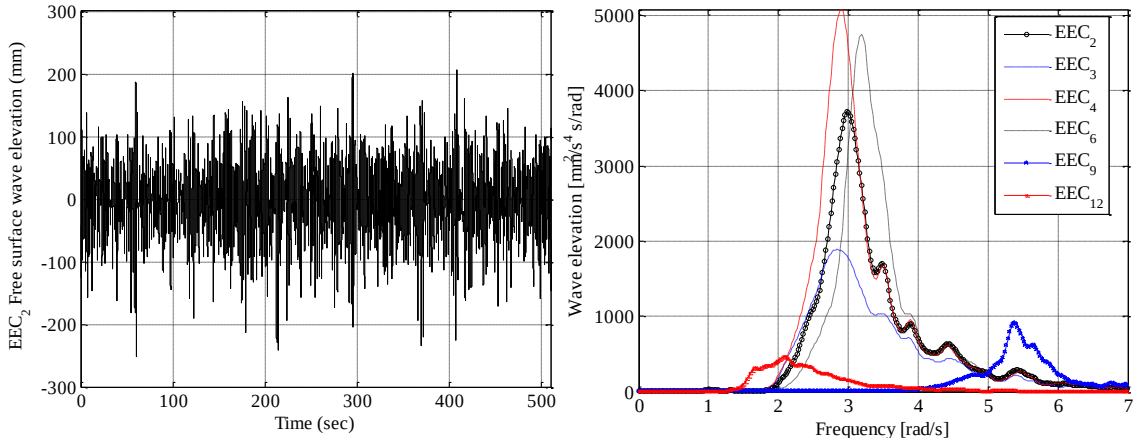

(a) (b)

Figure 12. Time series of the surface elevation for EEC_2 (Fig. 12a) and spectra (Fig. 12b) of the surface elevation for EEC_2, EEC_3, EEC_4, EEC_6, EEC_9 and EEC_{12}

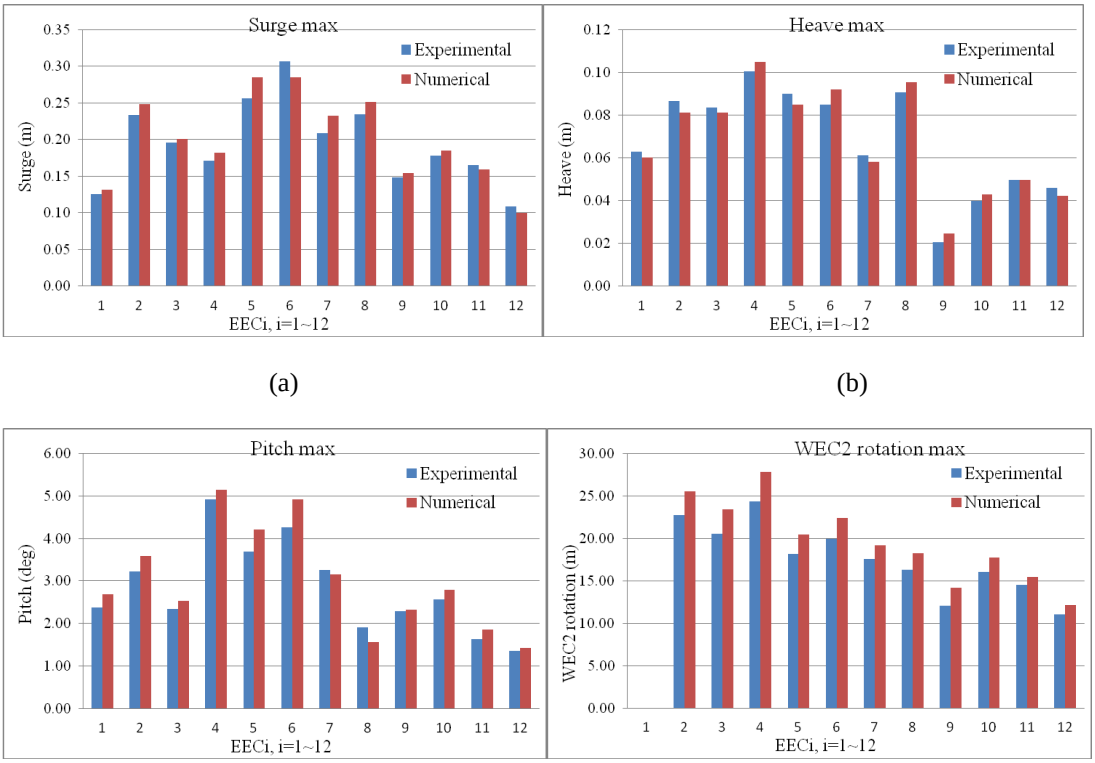

Figure 13. Statistical experimental and numerical max values of time series of surge (Fig. 13a), heave (Fig. 13b), pitch (Fig. 13c) and rotation of WEC2 (Fig. 13d) for EEC_i, i=1~12

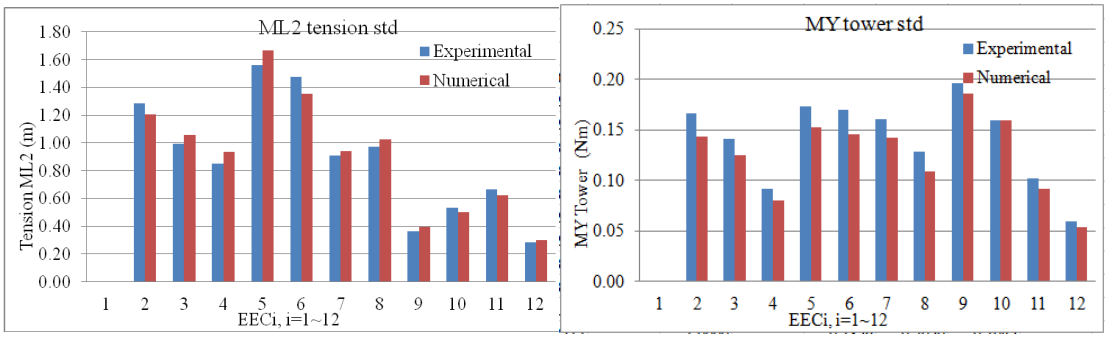

(a) (b)

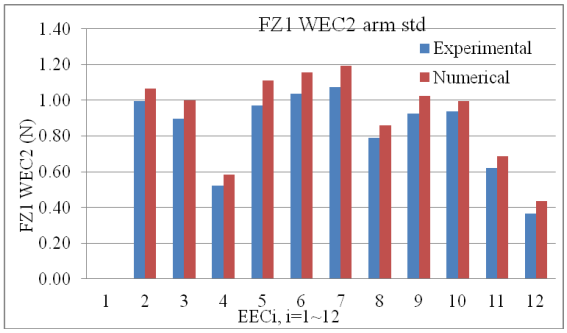

(c)

Figure 14. Comparison of statistical std value for EEC_i, i=1~12 of tension of ML2 (Fig. 14a), MY of tower (Fig. 14b) and FZ1 of WEC2 (Fig. 14c)

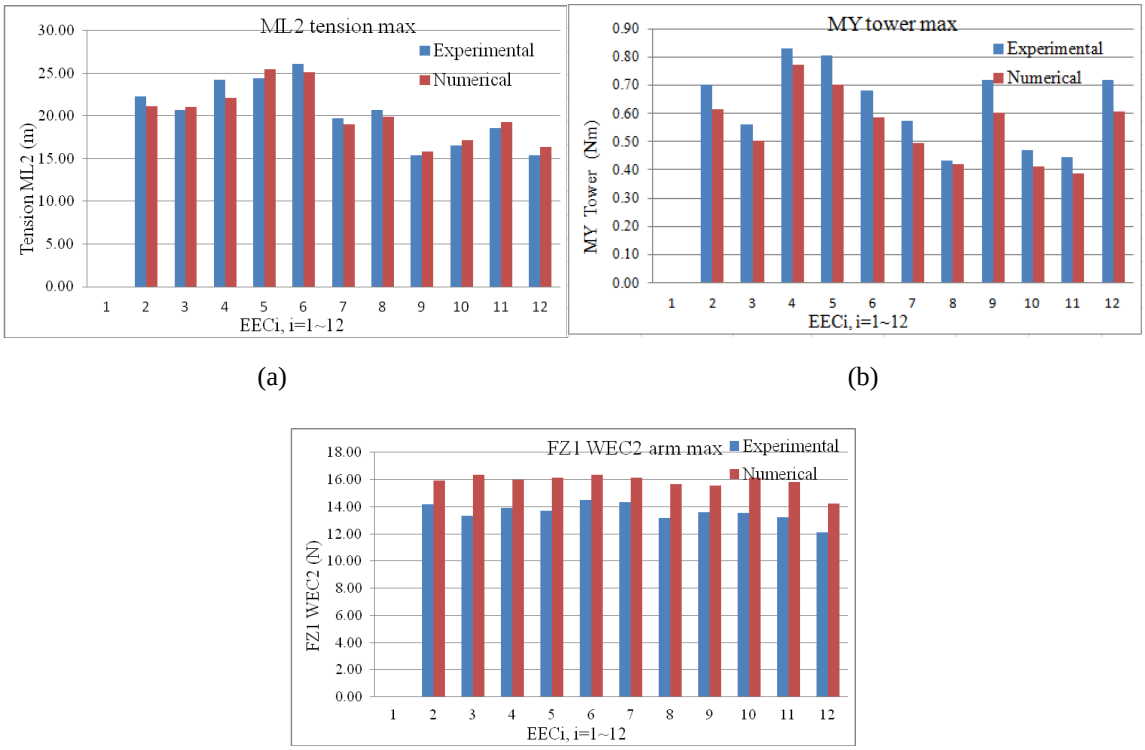

(a) (b)

(c)

Figure 15. Comparison of statistical max value for EEC_i, i=1~12 of tension of ML2 (Fig. 15a), MY of tower (Fig. 15b) and FZ1 of WEC2 (Fig. 15c)

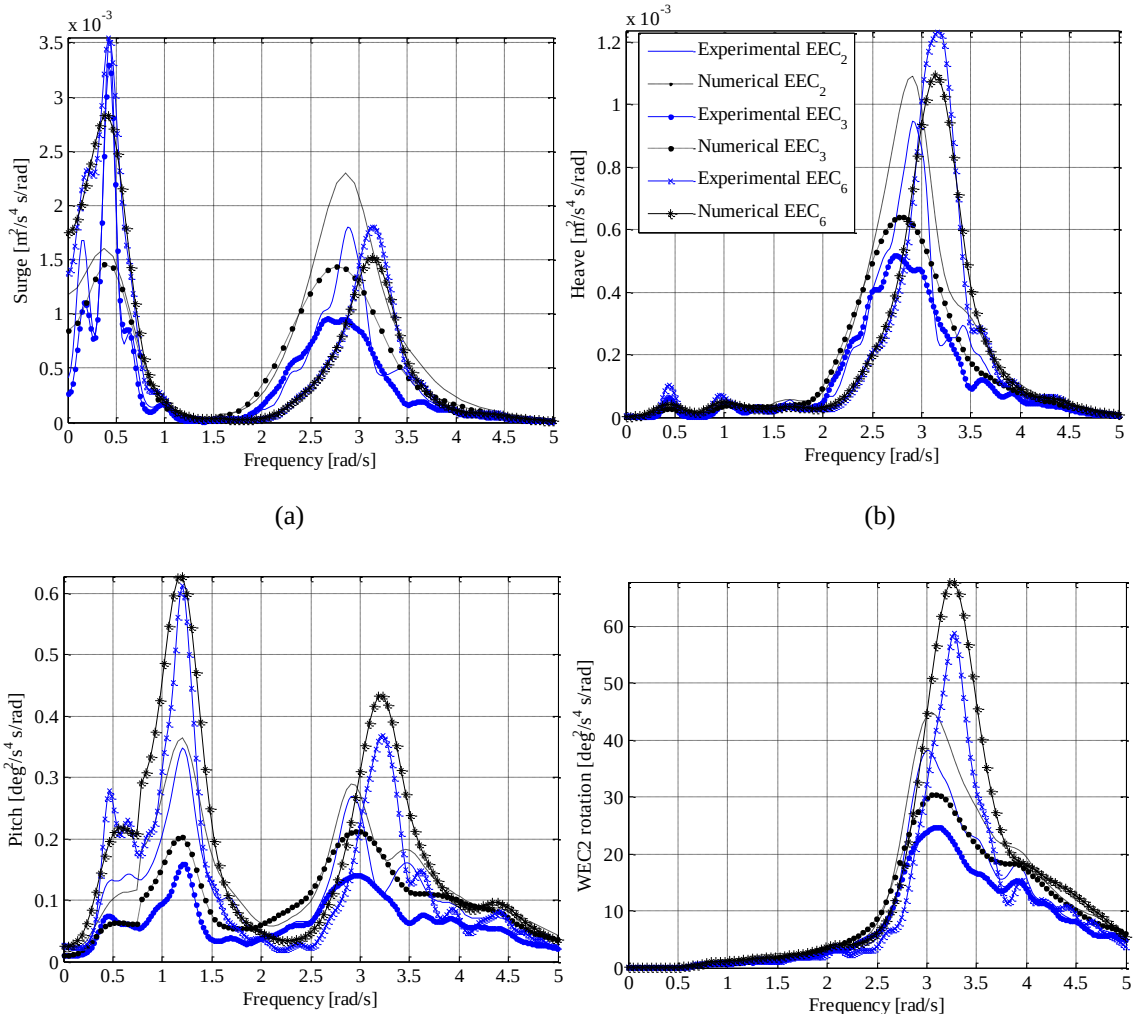

Figure 16. Comparison of spectra of surge (Fig. 16a), heave (Fig. 16b), pitch (Fig. 16c) and WEC2 rotation (Fig. 16d) between experimental and numerical results for EEC_2, EEC_3 and EEC_6

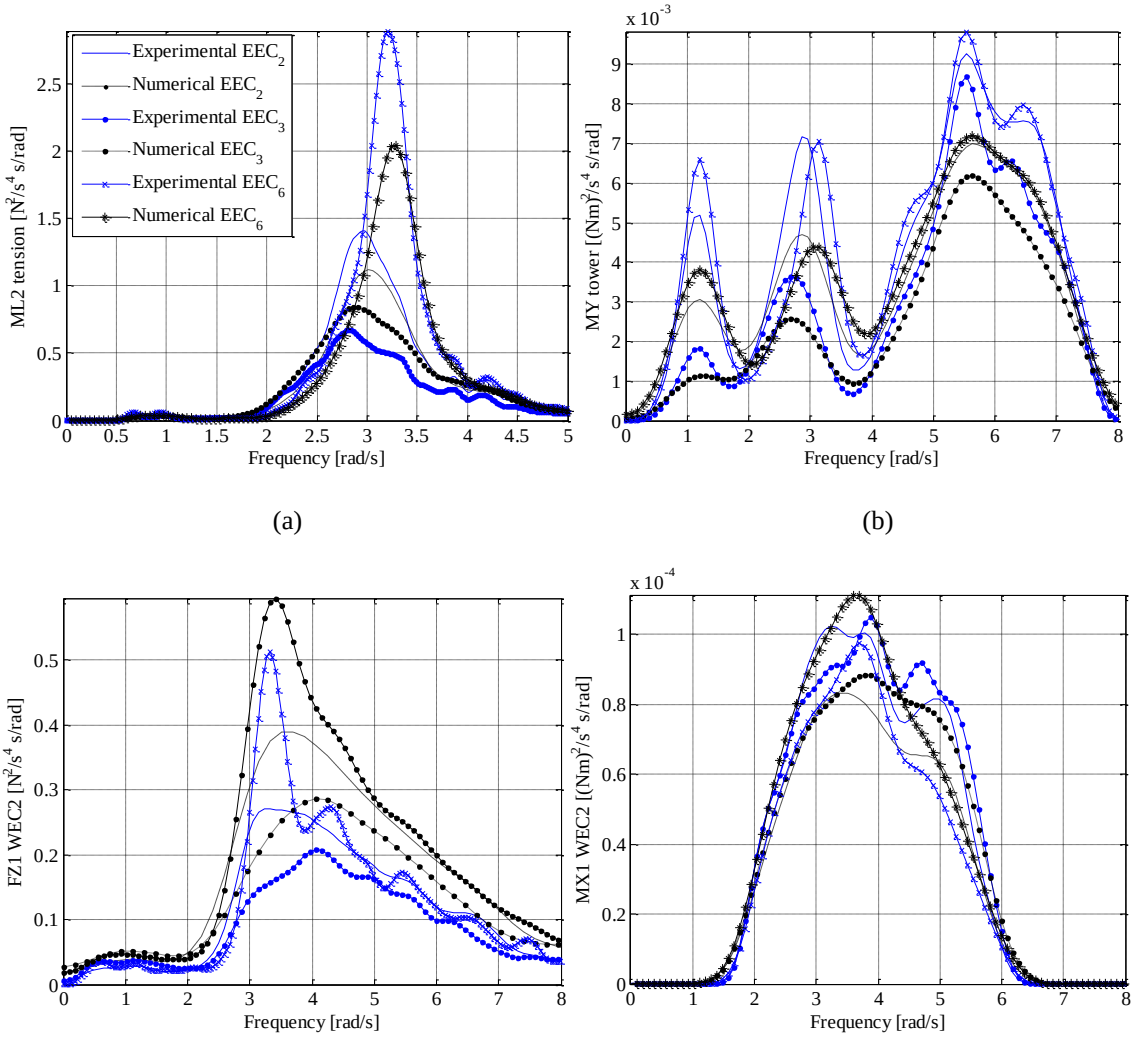

Figure 17. Comparison of spectra of tension of ML2 (Fig. 17a), MY of tower (Fig. 17b), FZ1 of WEC2 (Fig. 17c) and MX1 of WEC2 (Fig. 17d) between experimental and numerical results for EEC_2, EEC_3 and EEC_6

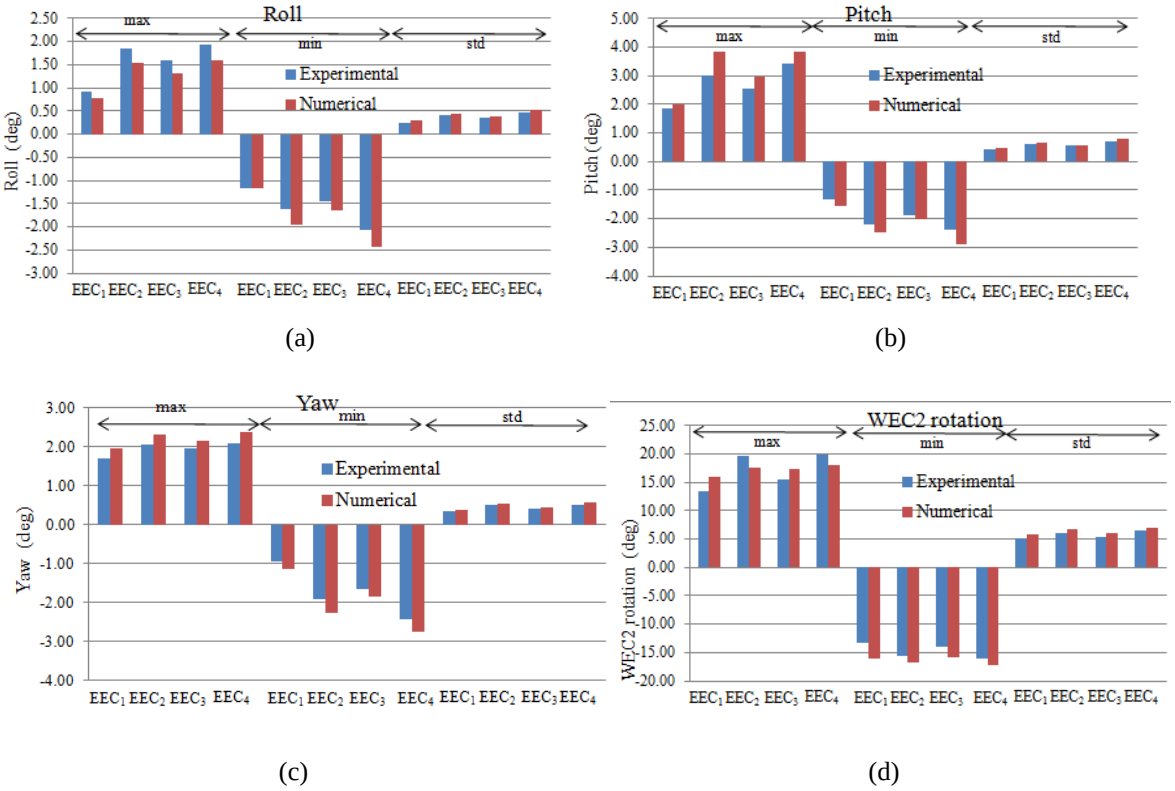

(a) (b)

(c) (d)

Figure 18. Statistical max, min and std values of roll (Fig. 18a), pitch (Fig. 18b), yaw (Fig. 18c) and rotation of WEC2 (Fig. 18d) for EEC_i, i=1~4 subjected to oblique wave and wind conditions

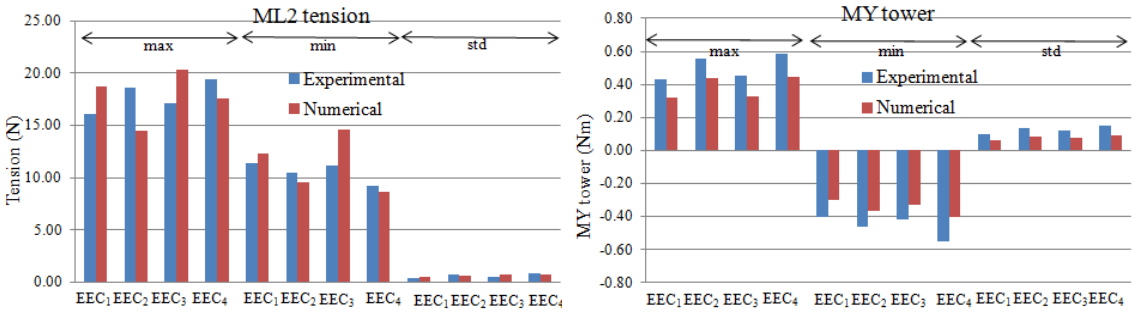

(a)

(b)

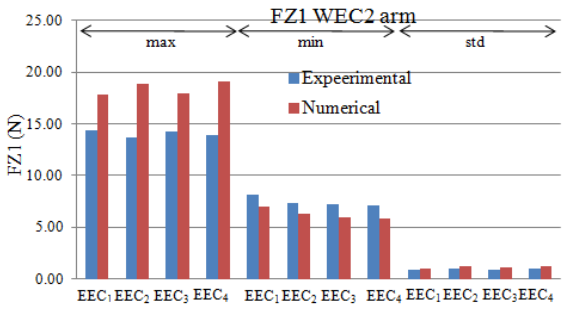

(c)

Figure 19. Statistical max, min and std values of ML2 tension (Fig. 19a), MY of tower (Fig. 19b) and FZ1 of WEC2 (Fig. 19c) for EEC_i, i=1~4, subjected to oblique wave with wind loading

Table 1. Scaling of different variables using the Froude laws of similitude

Variables	Scale factor	
Linear dimensions (length, height, width, wave height etc)	λ	50
Mass and force	λ^3	125,000
Time and velocity	$\lambda^{0.5}$	7.07
Moment	λ^4	6,250,000
Angular motion and acceleration	1	1

Table 2. Dimensions and characteristics of the main components of the SFC

Properties	Model scale value (Scale factor 1:50)	Properties	Model scale value (Scale factor 1:50)
Diameter of the center and outer columns [m]	0.130	Length of the flap[m]	0.400
Height of the pontoon [m]	0.120	Height of the flap [m]	0.140
Width of the pontoon [m]	0.180	Elliptical axis of flap [m]	0.070
Distance from the center line of the center column to the edge of the pontoon [m]	0.910	Mass of each flap [kg]	0.800
Draft [m]	0.625	Displacement of each flap [kg]	3.148
COG(x,y,z) [m]	(0,0,-0.498)	WEC Ix'x' local coordinate system ($kg*m^2$)	0.002
Ixx ($kg*m^2$)	23.515	WEC Iy'y' ($kg*m^2$)	0.014
Iyy ($kg*m^2$)	23.515	WEC Iz'z' ($kg*m^2$)	0.013
Izz ($kg*m^2$)	5.966	Wind turbine	Scaled NREL 5MW

Table 3. Structural properties of different parts of wind turbine in model scale

Variables	SFC
Blade length [m]	1.223
Blade mass [kg]	0.135
Nacelle mass [kg]	1.95
Shaft tilt [^{o}]	5
Hub mass [kg]	0.635
Vertical distance of hub to the MWL [m]	1.8
Horizontal distance of hub to the tower [m]	0.099
Tower mass [kg]	1.81
Diameter of tower [m]	0.022

Table 4. Numerical modelling methods that are used for different parts of SFC

Part of SFC	Mass model	Structural model	External load model
Semisubmersible platform	Integrated mass	Rigid body	• Gravity\Buoyancy • First and second order wave loads • Viscous force (distributed CD coefficients along the members of platform)
Three flaps	Integrated mass	Rigid body	• Gravity\Buoyancy • First order wave loads • Mean drift force
Mooring lines and arms of WECs	Distributed mass	Flexible body	• Gravity\Buoyancy • Morison formula
Tower	Distributed mass	Flexible body	• Gravity
Nacelle and hub	Integrated mass	Rigid body	• Gravity
Three blades	Distributed mass	Flexible body	• Gravity • Thrust measured wind loads

Table 5. Natural periods obtained from numerical and experimental decay tests

Degree of freedom	Initial offset* (m or deg)	T_{exp}* (sec)	T_{num}* (sec)	ε (%)	ξ_{exp}
$Surge_1$	0.458	16.13	15.912	1.35%	0.048
$Surge_2$	0.639	16.26	16.035	1.38%	0.042
$Surge_3$	0.745	16.23	16.354	0.76%	0.047
$Surge_4$	-0.256	15.82	15.945	0.79%	0.036
$Surge_5$	-0.378	15.63	15.922	1.87%	0.042
$Sway_1$	-0.276	14.67	15.375	4.81%	0.067
$Sway_2$	-0.308	14.78	15.382	4.07%	0.067
$Sway_3$	-0.270	14.83	15.375	3.67%	0.069
$Heave_1$	-0.128	3.69	3.77	2.17%	0.031
$Heave_2$	-0.078	3.76	3.73	0.80%	0.027
$Heave_3$	-0.084	3.74	3.74	0.00%	0.029
$Roll_1$	-2.757	4.77	4.73	0.84%	0.042
$Roll_2$	-2.259	4.70	4.71	0.21%	0.045
$Roll_3$	-3.579	4.75	4.76	0.21%	0.047
$Pitch_1$	4.715	4.97	4.92	1.01%	0.048
$Pitch_2$	5.588	4.83	4.94	2.28%	0.051
$Pitch_3$	4.040	4.92	4.91	0.20%	0.053
Yaw	4.050	-	7.05	-	-
WEC2 rotation	7.822	2.09	2.111	1.00%	0.057

* For full scale values multiply with the values in Table 1

Table 6. Examined wave periods for regular tests

Examined case	T_i (sec)	Ursell number	H/λ
T_1	0.709	0.000197	0.050966
T_2	0.847	0.000401	0.035711
T_3	0.985	0.000734	0.026406
T_4	1.122	0.001236	0.020351
T_5	1.260	0.001966	0.016137
T_6	1.398	0.002980	0.013109
T_7	1.536	0.004342	0.010859
T_8	1.673	0.006111	0.009153
T_9	1.811	0.008391	0.007811
T_{10}	1.949	0.011256	0.006744
T_{11}	2.087	0.014799	0.005882
T_{12}	2.224	0.019084	0.005180
T_{13}	2.362	0.024279	0.004592
T_{14}	2.500	0.030471	0.004099

Table 7. Examined extreme environmental conditions, EEC_i, i=1~12

EEC_i, i=1~12,	T_p (sec)	H_s (m)	U_w (m/sec)	TI
EEC_1	2.093	0.176	3.945	-
EEC_2	2.121	0.270	4.709	0.108
EEC_3	2.220	0.230	3.437	0.101
EEC_4	2.192	0.306	4.440	0.092
EEC_5	2.263	0.290	4.525	0.101
EEC_6	1.980	0.290	4.243	0.102
EEC_7	1.697	0.240	3.677	0.108
EEC_8	2.546	0.220	3.394	0.091
EEC_9	1.131	0.140	3.111	0.106
EEC_{10}	1.414	0.190	3.111	0.104
EEC_{11}	2.828	0.170	3.111	0.098
EEC_{12}	3.111	0.100	3.111	0.101

Table 8. Statistical std values of experimental and numerical results of surge, heave, pitch and rotation of WEC2 for EEC_i, i=1~12

Standard deviation												
	Surge (m)			Heave (m)			Pitch (deg)			WEC2 rotation (deg)		
EECi	Exp.	Num.	Rel. Diff.	Exp.	Num.	Rel. Diff.	Exp.	Num.	Rel. Diff.	Exp.	Num.	Rel. Diff.
EEC_1	0.0305	0.0326	7%	0.0175	0.0154	-12%	0.4834	0.5120	6%			
EEC_2	0.0497	0.0532	7%	0.0277	0.0255	-8%	0.7122	0.7250	2%	7.0903	7.7540	9%
EEC_3	0.0439	0.0506	15%	0.0240	0.0235	-2%	0.5869	0.6140	5%	6.4657	7.0570	9%
EEC_4	0.0610	0.0640	5%	0.0294	0.0298	1%	0.8412	0.8740	4%	6.7980	7.5570	11%
EEC_5	0.0554	0.0612	11%	0.0269	0.0248	-8%	0.8687	0.9120	5%	7.0808	8.0580	14%
EEC_6	0.0550	0.0515	-6%	0.0276	0.0254	-8%	0.8331	0.9150	10%	7.3495	8.1980	12%
EEC_7	0.0458	0.0524	14%	0.0197	0.0210	7%	0.7243	0.7015	-3%	7.2583	8.1600	12%
EEC_8	0.0460	0.0501	9%	0.0252	0.0275	9%	0.5754	0.5240	-9%	5.7187	6.2540	9%
EEC_9	0.0313	0.0315	1%	0.0058	0.0075	30%	0.4777	0.4980	4%	4.1873	4.5680	9%
EEC_{10}	0.0384	0.0412	7%	0.0110	0.0126	14%	0.5775	0.6240	8%	5.8601	6.1250	5%
EEC_{11}	0.0401	0.0346	-14%	0.0214	0.0220	3%	0.4818	0.5840	21%	4.5978	5.2450	14%
EEC_{12}	0.0221	0.0201	-9%	0.0134	0.0125	-6%	0.3099	0.3150	2%	3.2200	3.8060	18%